Dopingless Negative Capacitance Ferroelectric TFET for Breast Cancer Cells Detection: Design and Sensitivity Analysis

Shradhya Singh and Sangeeta Singh, *Member, IEEE*

***Abstract*— The current research article reports the electrical detection of breast cancer cell lines (MDA-MB-231, Hs578T, T47D, and MCF-7) by deploying dopingless negative capacitance (NC) ferroelectric (FE) tunnel field-effect transistor (DL-FE-TFET). This device has a double dual metal gate and two nanocavities engraved underneath both gate electrodes for higher detection sensitivity. Our work reports the detection of nontumorigenic cell (MCF-10A) and breast cancer cell lines by combining the NC effect of FE material and dopingless technology synergistically. Here, FE material amplifies the applied gate bias intrinsically. The in-depth electrostatic analysis in terms of surface potential, carrier concentration, energy band diagram, drive current, and electric field has been depicted. Variation of the dielectric constant of these breast cancerous cell lines dictates the detection mechanism in our reported biosensor. The sensitivity has been analyzed in terms of drive current, I_{ON}/I_{OFF} ratio, V_{th}, and transconductance. The optimized cavity structure demonstrates significantly high drain current sensitivity of the order of 2.88×10^9 and I_{ON}/I_{OFF} ratio sensitivity of the order of 3.2×10^5. In addition, the effect of device geometry variation, such as cavity length and FE layer thickness on the drain current sensitivity and I_{ON}/I_{OFF} sensitivity, transconductance sensitivity (S_{g_m}), and threshold voltage sensitivity ($S_{V_{th}}$) of the device, has also been investigated. This device structure may be deployed for the array-based screening and diagnosis of breast cancer cells lines, with additional benefits including a simpler mechanism of transduction, cost effectiveness, technology compatibility with CMOS process, adjustable electrical response, and reproducibility.**

***Index Terms*— Breast cancer, cell lines, dielectric-modulated TFET, ferroelectric (FE), negative capacitance (NC).**

I. Introduction

THE increased mortality rate due to cancer is one of the significant concerns worldwide. Cancer is not a disease caused by foreign organisms but due to specific genetic mutations in cells or tissues. Such cells do not function normally but rather divide and multiply recalcitrantly, forming a mass of mutated tissue called a tumor. Cancer is classified according to the type of cell that causes it and where it originates. Due to their high occurrence rate, breast, colorectal, and lung cancers are the most prevalent cancer types that are well-known around the world. Among women, one of the most commonly diagnosed cancers is breast cancer. It consists of about 11.6% of all cancer diagnosed and 6.6% of deaths due to cancer globally in 2018 [1]. Timely diagnosis of cancer can help in the effective treatment and reduction in death rate. Currently, the primary tool that is used for breast cancer detection is X-ray mammography. Although this method achieved huge progress in this field, it has also been reported with several limitations [2]–[4]. However, for dense breasts, sensitivity and specificity of the X-ray mammography reduce significantly to 67% and 89%, respectively [5], [6]. Furthermore, magnetic resonance imaging (MRI) with enhanced contrast has better sensitivity, ranging from 93% to 100% [7]; however, this technology is cumbersome, expensive, and hospital-based. In contrast to X-ray mammography, ultrasonography requires a skilled operator and has also been reported with an elevated rate of false positives [8]. In addition, women residing in geographically remote regions do not have smooth access to diagnostic facilities of high quality. Even in the developed countries, due to rising health care treatment cost, there is an urgent requirement of a diagnostic technique that is robust, easy to interpret, and cost-effective [9].

The microwave imaging technology was developed to address the limitations of traditional imaging. At a range of microwave frequencies, this approach relies on a considerable dielectric differential between normal and malignant tissues [10]–[14]. On microwave radiation, malignant breast tissues with a high water content scatter more than normal tissues having lesser water content. It was observed the varying density of breast tissues, and the contrast in electric permittivity of healthy and cancerous tissues is between 2:1 [15], [16]. Previously reported literature fetches the dielectric properties of normal as well as cancerous breast tissues. Furthermore, the dielectric properties of malignant, fibro, and fatty glandular breast tissues were computed with the range of frequency as 50 MHz–5 GHz using a two-port sample holder and an open-ended coaxial probe. It was observed that the dispersion characteristic of cancerous tissues is unlike normal breast

Manuscript received November 12, 2021; accepted December 12, 2021. Date of publication December 15, 2021; date of current version March 3, 2022. *(Corresponding author: Sangeeta Singh.)*

The authors are with the Microelectronics and VLSI Laboratory, National Institute of Technology at Patna, Patna 800005, India (e-mail: shradhyas.phd18.ec@nitp.ac.in; sangeeta.singh@nitp.ac.in).

Digital Object Identifier 10.1109/TUFFC.2021.3136099

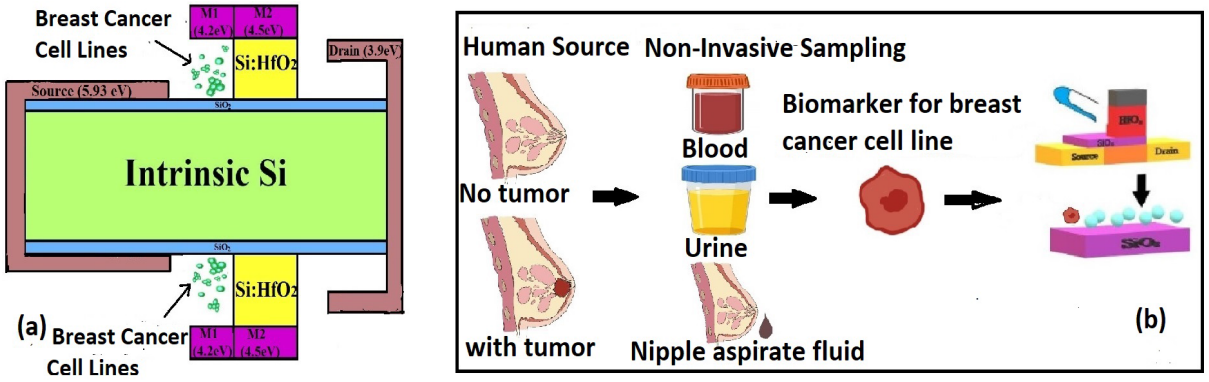

Fig. 1. (a) 2-D schematic (b) breast cancer cell lines immobilization of DL-FE-TFET-based biosensor for breast cancer cell lines detection.

TABLE I
DIFFERENT BREAST CANCER CELLS WITH ITS DIELECTRIC CONSTANTS (*K*) MEASURED AT 230-MHz FREQUENCY [24]

Breast cancer cell lines	Dielectric constant (K)
MCF-10A	4.5
HS578t	22
MDA-MB-231	24.5
MCF7	27.5
T47D	32

TABLE II
SIMULATION PARAMETERS FOR DL-FE-TFET-BASED BIOSENSOR DEVICE

Parameters	Values
Silicon thickness (t_{Si})	10 nm
Gate oxide thickness (t_{ox})	0.5 nm
Ferroelectric oxide thickness (t_{FE})	3 nm
Gate length (L_G=L_1+L_2)	20 nm+30 nm
Source length (L_S)	100 nm
Drain length (L_D)	100 nm
Background doping (N_{in})	$1 \times 10^{16} cm^{-3}$
Source work-function (ϕ_S(Pt))	5.93 eV
Drain work-function (ϕ_D (Hf))	3.9 eV
Cavity thickness	(h_c) 3 nm
Gate metal1 Work function (ϕ_{M1})	4.2 eV
Gate metal2 Work function (ϕ_{M2})	4.5 eV

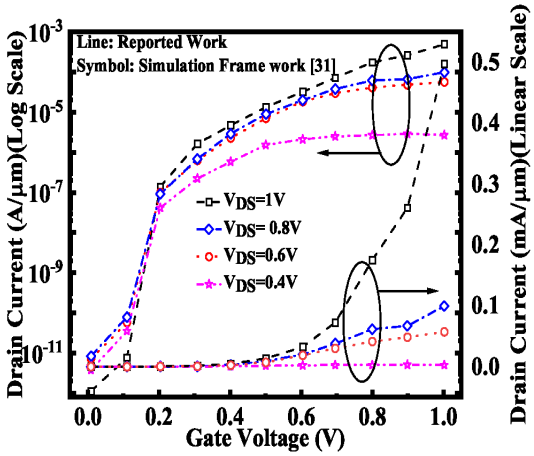

Fig. 2. Calibration of the device characteristics of dopingless FE TFET device's simulated drain current with FE TFET.

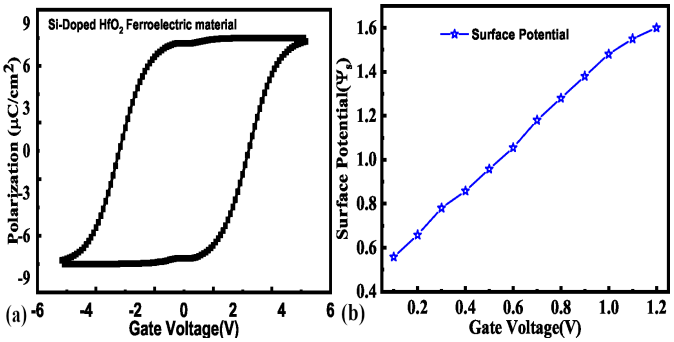

Fig. 3. (a) *P*–*V* hysteresis curve of the MOS capacitor by considering Si doped HfO_2 FE material as gate oxide and (b) surface potential as a function of gate-to-source applied bias.

tissue [17]. The dielectric properties of the human tissues measured from the frequency range of 50–900 MHz and reported that both permittivity and conductivity are more for cancerous tissues unlike the normal tissues of the same type [18]. In the previously reported literature, dielectric characteristics corresponding to various *in vitro* breast cancerous cell lines have been studied using the open-ended coaxial probe technique ranging from 200 MHz to 13.6 GHz. It includes a nontumorigenic healthy (MCF-10A) and breast cancerous cell lines (MDA-MB-231, Hs578T, T47D, and MCF-7). Moreover, with the correct knowledge of the dielectric constant of human breast tissues at different microwave frequencies, it is possible to effectively implement breast cancer cell detection with a dielectric-modulated TFET device as the best measure for early diagnosis.

This work reports the detection of breast cancer cell lines from its dielectric constant value by utilizing dopingless dual negative capacitance (NC) FE tunnel field-effect transistor (DL-NC-FE-TFET)-based device. For enhancing the detection sensitivity, this device incorporates a double dual metal gate and two nanocavities carved beneath both gate electrodes. By combining the NC effect of FE material and dopingless technology, it detects nontumorigenic cells (MCF-10A) and breast cancer cell lines. TFET devices are the better alternative to CMOS technology-based biosensors due to its inherent phenomenon of band-to-band tunneling and it also has a lower leakage current and subthreshold slope (SS) below

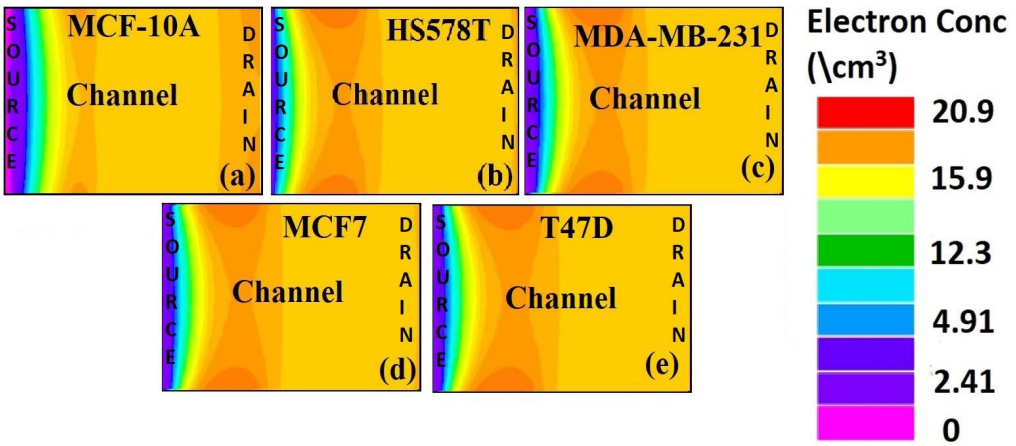

Fig. 4. Electron concentration contour in channel region for healthy nontumorigenic. (a) MCF-10A and breast cancer. (b) MDA-MB-231. (c) Hs578T. (d) T47D. (e) MCF-7 cell lines immobilized in cavity region.

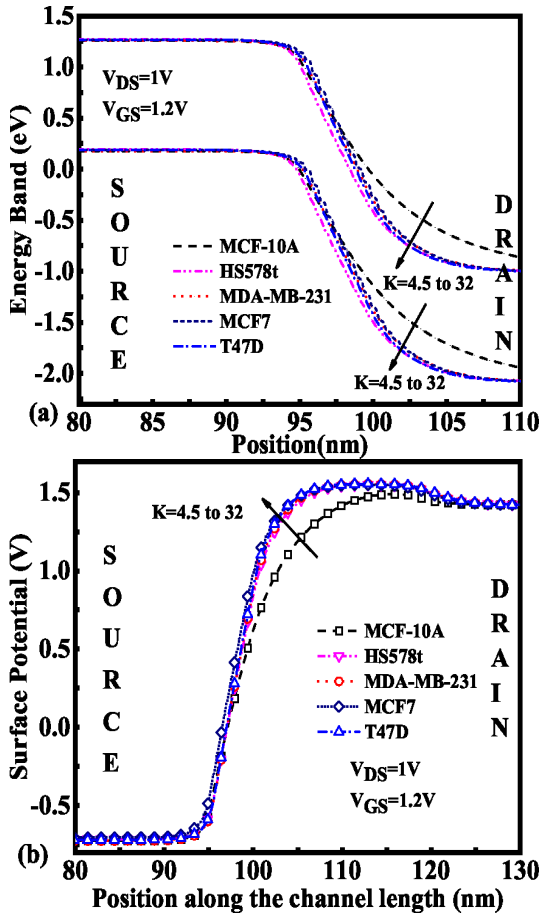

Fig. 5. (a) Energy band diagram and (b) surface potential of DL-FE-TFET-based biosensor with respect to the device length at varying dielectric constant of different breast cancerous cell lines.

Boltzmann's limit (<60 mV/decade) [19], [31]–[34]. Amplification of low gate voltage by utilizing NC would empower the low-power operation. In this study, Si-doped HfO_2 FE material has been utilized as gate-stack to introduce the NC effect in the device [20]. In addition to this, due to random dopant fluctuations (RDFs), it is critical for achieving a sharp doping profile (i.e., essential for band-to-band tunneling) toward the source–channel and the drain–channel junction. These shortcomings and fabrication complexity can be overcome by avoiding metallurgical doping [21], [22]. Hence, the dopingless technique has been developed to form the source and drain region in TFET by employing a suitable electrode metal work function on either side [22], [23], [25]. Furthermore, the dual material gate technique is utilized as the higher work function of gate metal (M2) placed toward drain side and the lower work function of metal (M1) toward the source side to enhance the drive characteristic [28]. The proposed structure detects breast cancer cell lines with two etched nanocavities in the gate dielectric. The dielectric constant of four different breast cancer cell lines (MCF-7, MDA-MB-231, HS578T, and T47D) and a normal cell line (MCF-10A) was measured at the frequency 230 MHz reported in [24], as stated in Table I.

This article is organized as follows. Section II includes structure and simulation models. Section III shows the results and discussions along with the sensitivity analysis. Finally, Section IV concludes the study.

II. Device Architecture and Simulation Approach

A dopingless dual metal gate FE tunnel field-effect transistor (DL-FE-TFET)-based biosensor structure has been reported for the detection of breast cancer cell lines. There are several benefits of utilizing this structure in terms of steep SS, low power, and easier fabrication process. The 2-D schematic of the reported DL-FE-TFET-based breast cancer cell lines detector and the process of immobilization within the cavity region are shown in Fig. 1(a) and (b), respectively. All the structural parameters of the device are labeled in Fig. 1. The proposed structure resembles a double-gate structure with the dual underlap cavity underneath gate metal as the binding site for the immobilization of the breast cancer cell lines with the effect of the dielectric modulation approach. A SiO_2 layer grown over the Si film is considered a native oxide layer, which acts as an adhesion layer for the cell lines. Furthermore, Si-doped HfO_2 FE material is grown over the SiO_2 layer as

Fig. 6. Surface potential contour of DL-FE-TFET-based biosensor for (a) nontumorigenic (MCF-10A) and (b) breast cancerous cell lines (MDA-MB-231).

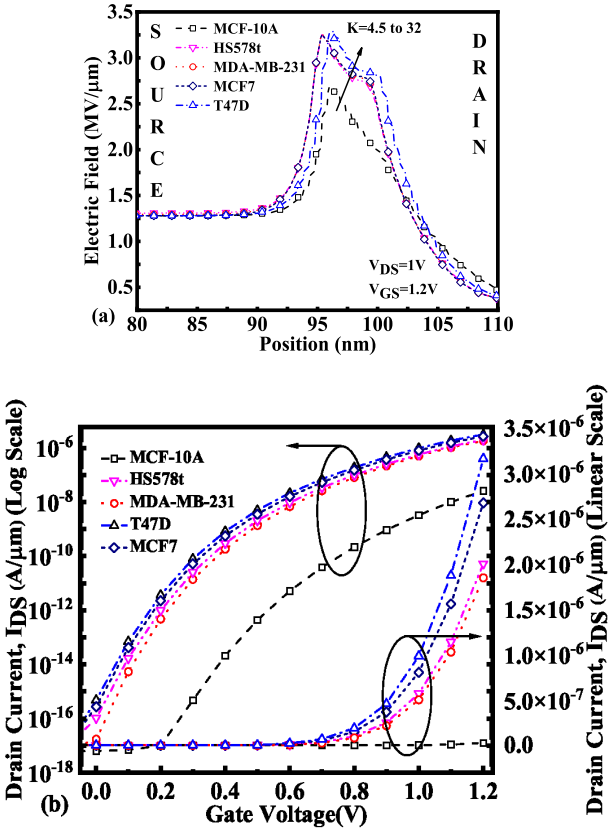

Fig. 7. (a) Electric field and (b) I_D–V_{GS} characteristic of DL-FE-TFET-based biosensor at varying dielectric constant of different breast cancerous cell lines.

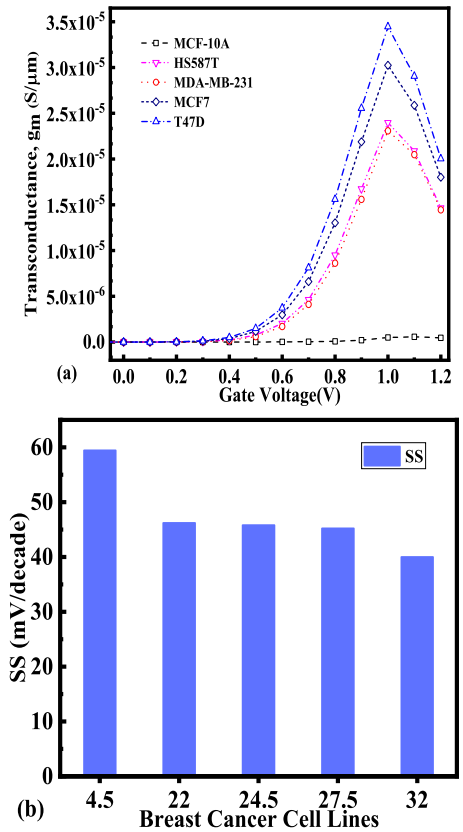

Fig. 8. (a) Transconductance and (b) SS of DL-FE-TFET-based biosensor at different values of dielectric constant of different breast cancerous cell lines.

a gate-stack to amplify the low gate voltages to empower the low power application. The crucial FE material properties of Si:HfO_2 considered for the proposed structure simulations are coercive field (F_C), remanent polarization (P_r), saturation polarization (P_s), and the dielectric constant of doped Si:HfO_2 (FE) are considered to be 2 MV/cm, 1 μC/cm^2, 20 μC/cm^2, and 31, respectively, [25]. To overcome several fabrication issues that arise with metallurgical doping, the dopingless technique is utilized to form source and drain regions. It is realized by applying appropriate metals with suitable work functions such as Hf (3.9 eV) and Pt (5.93 eV) for the formation of drain and source regions, respectively, [27]. The dual metal chosen as gate electrode with work function of M1 and M2 is as $\phi_{M1} = 4.2$ eV and $\phi_{M2} = 4.5$ eV, respectively, [27]. The detailed device dimensional parameters considered are listed in Table II.

During the fabrication of the DL-FE-TFET-based biosensor structure, the cavity region is developed in gate dielectric toward the source region by dry etching. A thin SiO_2 layer is grown by dry oxidation on the Si film in the cavity region, which serves as an adhesive layer for bioanalytes. Metallization of the drain, source, and gate regions is performed by low-pressure chemical vapor deposition (CVD) [27]. The performance measurement of DL-FE-TFET-based biosensor is done by immobilizing the cavity region completely with different breast cancerous cell lines. It includes nontumorigenic cell line (MCF-10A) and breast cancerous cell lines (MDA-MB-231, Hs578T, T47D, and MCF-7). To study the

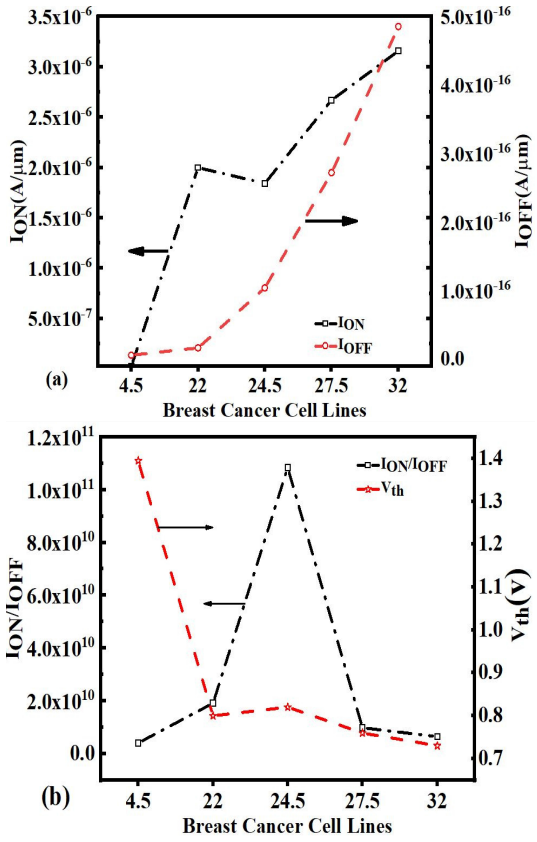

Fig. 9. (a) I_{ON} and I_{OFF} and (b) I_{ON}/I_{OFF} and V_{th} of DL-FE-TFET-based biosensor at varying dielectric constant of different breast cancerous cell lines.

breast cancer sensing behavior of the reported biosensor, the impact of the filled cavity with breast cancerous cell lines (MDA-MB-231, Hs578T, T47D, and MCF-7) with a higher dielectric constant on electrical performance characteristics is analyzed in reference to the healthy nontumorigenic, MCF-10A ($K = 4.5$). The dielectric constants of all the breast cancer cell lines are mentioned in Table I. According to the existing works in detecting various breast cancer cell lines, nanoparticles (NPs) have been utilized, which is of size below 10 nm [34]–[37]. To examine the biosensor performance of the proposed structure, ATLAS TCAD SILVACO tool [28] has been utilized. In order to achieve the accurate simulation of device parameters, appropriate models have been induced in the simulator. Here, a nonlocal band-to-band tunneling model (BTBT model) has been utilized to enable the measurement of the tunneling rate toward the tunneling junction. For the L-K equation modeling, LKNC is also included in the models. To incorporate the mobility dependence on the field and concentration, the CVT model is invoked. To achieve the carrier recombination, the Shockley–Read–Hall (SRH) model is chosen. The bandgap narrowing (BGN) model is incorporated to enable the high concentration impact on the bandgap. The Fermi–Dirac statistics model is included to incorporate the property changes of a highly doped region. Fig. 2 shows the calibration of transfer characteristics with earlier FE state of the art [22], which represents a good agreement with our simulation framework. In order to get better insight of the NC effect, Fig. 3(a) represents the polarization variation with gate voltage, i.e., P–V hysteresis curve of the MOS capacitor by considering Si-doped HfO_2 FE material as gate oxide. From the P–V curve, the coercive field of Si-doped HfO_2 has been calculated as 2.6 MV/cm. Furthermore, to present the intrinsic voltage amplification behavior, the surface potential is plotted as a function of V_{GS} in Fig. 3(b).

III. Result and Discussion

Our work utilizes the dielectric constant of different breast cancer cell lines measured at 230-MHz frequency reported in [24] and listed in Table I. By utilizing the concept of dielectric modulation technique with the reported DL-FE-TFET-based biosensor, detection of various breast cancerous tissues is investigated in this section.

A. Dielectric-Modulated Electrostatic Analysis for Breast Cancer Cell Lines

The charge carriers concentration contours of the proposed device for nontumorigenic cell lines (MCF-10A) and breast cancer cell lines (MDA-MB-231, T47D, Hs578T, and MCF-7) immobilized within the nanocavities are shown in Fig. 4. It is found that the required carrier concentration profile is achieved by deploying dopingless technique to realize the p^+-i-n^+ region for each cell line immobilized in the binding site of the proposed device. It is also noticed that with an increase in dielectric constant (in reference to different breast cancerous cell lines immobilized in cavity region), charge carrier concentration also increases under the cavity, as shown in Fig. 4(a)–(e). Due to the double-gate structure considered, the tunneling rates are identical for both interfaces. The tunneling rate G_{BTBT} in the TFET structure is the function of local electric field (E_F) as per the equation shown [28]

$$G_{BTBT} = AE^{\sigma}\exp\left(-\frac{B}{E}\right). \quad (1)$$

In (1), constant A depends on the electron's effective mass, B represents the tunneling probability constant, and σ indicates the transition constant. The impact of dielectric constant of immobilized breast cancerous cell lines in the cavity region on energy band diagram for ON state is shown in Fig. 5(a) ($V_{GS} = 1.2$ V and $V_{DS} = 1$ V). The increase in the dielectric constant of cell lines in the cavity region begins the immobilization process, which leads to the downward bending of the energy bands as shown in the figure. While shifting of both the bands leads to reduction of the barrier width toward source–channel junction and also improves the electron tunneling, the shifting in the valence band of the source region and conduction band of the channel region depends on the fluctuation in flat-band voltage. This fluctuation relies on the different dielectric constant of breast cancer cell lines immobilized in the cavity region. It is noted that the increase in dielectric constant values (i.e., from $K = 4.5$ to 32) in the cavity region leads to a rise in the surface potential at the source–channel junction [see Fig. 5(b)]. The increased abruptness of the junction profile and binding site underneath the gate electrode leads to the variation in surface potential shown in Fig. 5(b).

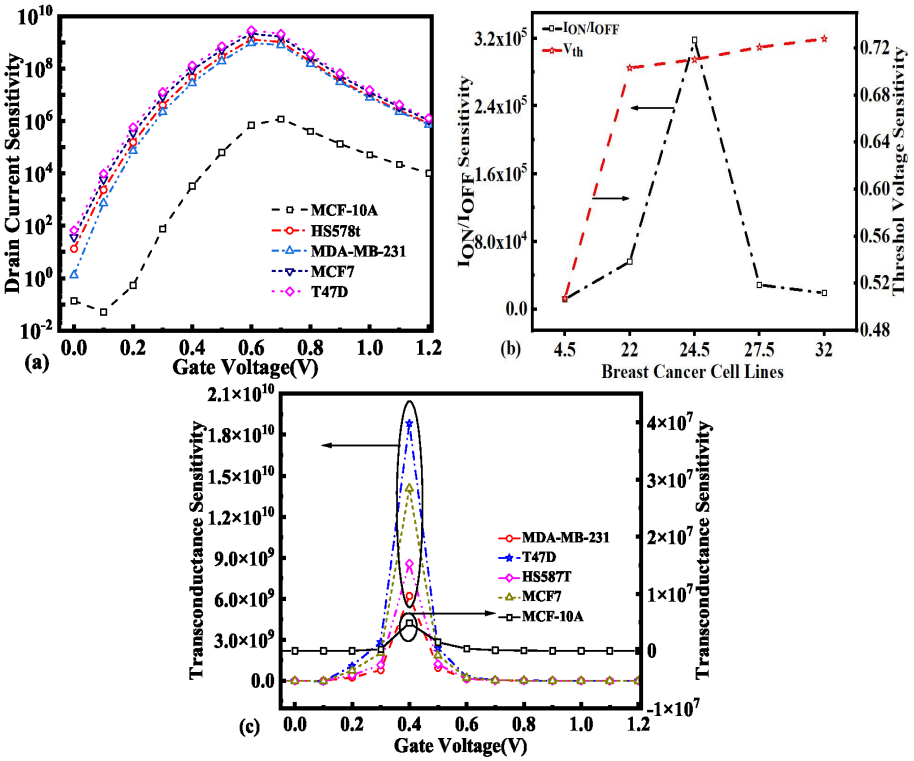

Fig. 10. (a) Drain current sensitivity, (b) I_{ON}/I_{OFF}, and (c) transconductance sensitivity of DL-FE-TFET-based biosensor by varying the dielectric constant of different breast cancerous cell lines.

The surface potential contour of DL-FE-TFET-based biosensor for nontumorigenic cell line (MCF-10A) and breast cancerous cell lines (MDA-MB-231) into the channel region is shown in Fig. 6. Increased surface potential can be noted for MDA-MB-231 compared to MCF-10A. Fig. 7(a) shows the variation in the electric field toward channel region due to different breast cancer cell lines immobilized in the cavity region. A rise in the K value of different cancerous cell lines results in increase in the electric field due to the enhanced capacitance coupling from gate to channel region. Fig. 4 shows the carrier concentration variation under the cavity region with the increasing dielectric constant of the bioanalyte to be detected. Higher capacitive coupling can be achieved for the bioanalytes with greater K values. Thus, higher carrier concentration can be achieved under the cavity region near the source–channel junction.

As the different breast cancer cell lines are immobilized into the cavity region, it results in an enhanced coupling between the gate metal and the channel region, and hence, the drive current increases. Also, surface potential improvement results in enhancement of the device ON current, as shown in Fig. 7(b). The transconductance with the variation in different dielectric constants of immobilized breast cancer cell lines in the cavity is shown in Fig. 8(a). The peak transconductance increases with an increase in the dielectric constant of cell lines. Furthermore, the impact on SS with the variation in dielectric constant is shown in Fig. 8(b). The SS decrease with a rise in the dielectric constant corresponds to breast cancer cell lines. The SS for breast cancer cell line T47D ($K = 32$) is 40 mV/decade and SS for healthy nontumorigenic MCF-10A ($K = 4.5$) is 59.5 mV/decade, whereas the SS for air ($K = 1$) in cavity is 82.5 mV/decade. Fig. 9(a) shows the variation in I_{ON} and I_{OFF} of the reported DL-FE-TFET with different breast cancer cell lines immobilized in the cavity region. It is found that the rise in dielectric constant leads to an increase in both I_{ON} and I_{OFF}. The maximum I_{ON} is achieved for breast cancer cell line T47D ($K = 32$) as 3.15×10^{-6} A/μm, whereas healthy nontumorigenic MCF-10A ($K = 4.5$) is achieved as 2.6×10^{-8} A/μm. Here, the maximum I_{OFF} is achieved as 4.8×10^{-16} A/μm for T47D ($K = 32$). Variation in I_{ON}/I_{OFF} ratio and threshold voltage with different breast cancer cell lines is shown in Fig. 9(b). It is noted that the maximum I_{ON}/I_{OFF} ratio is 1.08×10^{11} of MDA-MB-231 breast cancer cell line. Threshold voltage decreases with the rise in dielectric constant, as a high dielectric constant leads to the enhanced carrier concentration in the channel region. Hence, a lower gate voltage is required to turn ON the device. Therefore, the threshold voltage of the proposed device for healthy nontumorigenic MCF-10A ($K = 4.5$) is 1.39 V, and the minimum threshold voltage achieved as 0.73 V for breast cancerous cell line T47D ($K = 32$).

B. Dielectric-Modulated Sensitivity Analysis for Breast Cancer Cell Lines

The sensitivity analysis of DL-FE-TFET-based biosensor structure has been done in this section. To study the sensing behavior of the reported structure, the impact of the filled cavity with nontumorigenic cell line (MCF-10A) and breast cancer cell lines (MDA-MB-231, Hs578T, T47D, and MCF-7)

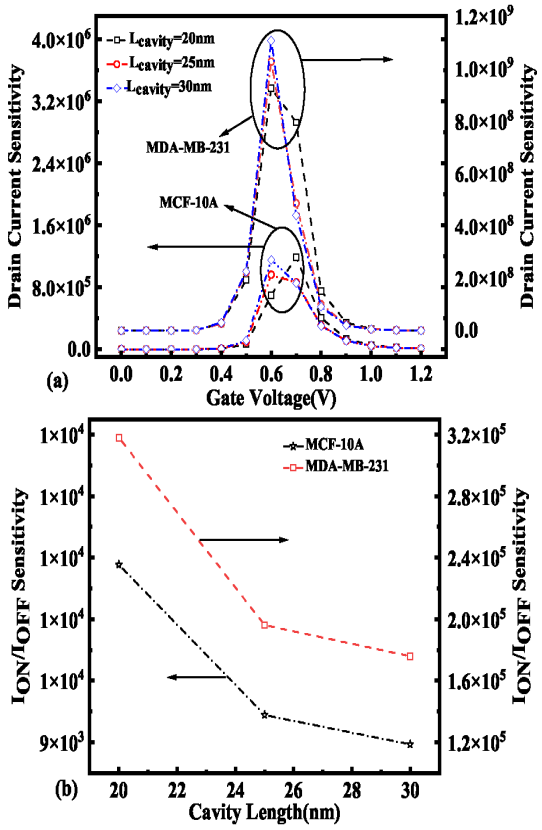

Fig. 11. Impact of cavity length variation on (a) drain current sensitivity and (b) I_{ON}/I_{OFF} sensitivity of DL-FE-TFET-based biosensor for nontumorigenic (MCF-10A) and cancerous cell (MDA-MB-231).

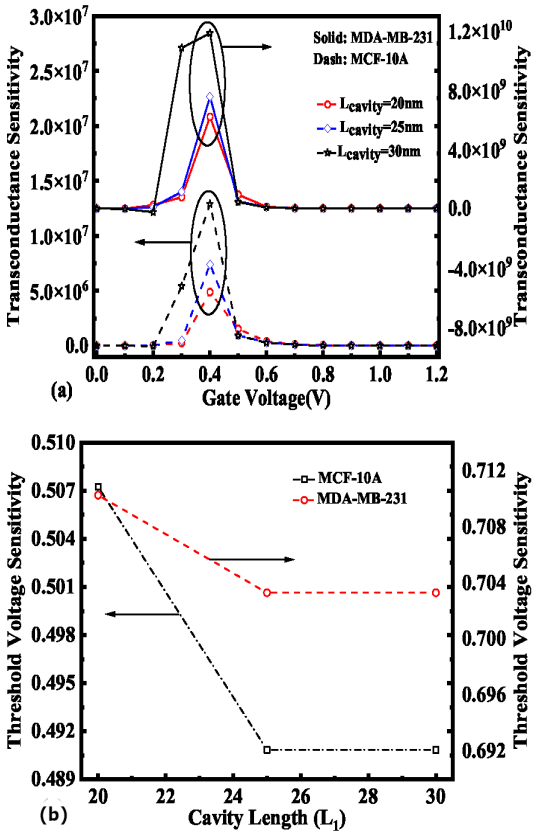

Fig. 12. Impact of cavity length variation on (a) transconductance sensitivity and (b) threshold voltage sensitivity of DL-FE-TFET-based biosensor for nontumorigenic (MCF-10A) and cancerous cell (MDA-MB-231).

on the electrical performance characteristics is analyzed in reference to the vacant cavity ($K = 1$, i.e., air). Therefore, the sensitivity analysis of the proposed sensor structure is done with the variation in drive current, I_{ON}/I_{OFF} ratio, V_{th}, and transconductance with reference to air in the cavity region. The mathematical formulation that has been considered to evaluate the sensitivities of the proposed structure in terms of various factors are [22]

$$S_{I_D} = \left(\frac{I_D(\text{CL}) - I_D(\text{air})}{I_D(\text{air})}\right) \tag{2}$$

$$S_{I_{ON}/I_{OFF}} = \left(\frac{I_{ON}/I_{OFF}(\text{CL}) - I_{ON}/I_{OFF}(\text{air})}{I_{ON}/I_{OFF}(\text{air})}\right) \tag{3}$$

$$S_{V_{th}} = \left(\frac{V_{th}(\text{CL}) - V_{th}(\text{air})}{V_{th}(\text{air})}\right) \tag{4}$$

$$S_{g_m} = \left(\frac{g_m(\text{CL}) - g_m(\text{air})}{g_m(\text{air})}\right). \tag{5}$$

In (2), $I_D(\text{CL})$ represents the drain current corresponding to the completely filled cavity with different healthy and cancerous cell lines and empty cavity yields the drain current as $I_D(\text{air})$ with $K = 1$. Fig. 10(a) shows the sensitivity of the proposed structure in terms of drain current sensitivity (S_{I_D}) for different cancerous cell lines and also healthy cell lines. The maximum drain current sensitivity achieved is 2.88×10^9 for T47D breast cancer cell lines at $V_{GS} = 0.6$ V. Sensitivities in terms of I_{ON}/I_{OFF} ($S_{I_{ON}/I_{OFF}}$) ratio and threshold voltage ($S_{V_{th}}$) are shown in Fig. 10(b). It is found that sensitivity in terms of $S_{I_{ON}/I_{OFF}}$ achieved the maximum value as 3.2×10^5 for MDA-MB-231 ($K = 24.5$) and sensitivity in terms of $S_{V_{th}}$ increases with the variation in dielectric constant of breast cancer cell lines. The maximum value achieved for $S_{V_{th}}$ is 0.72 for T47D ($K = 32$). Finally, the sensitivity in terms of transconductance (S_{g_m}) is shown in Fig. 10(c). It is noted that the sensitivity of healthy, nontumorigenic cell line, MCF-10A has a lesser sensitivity of 4.8×10^6 compared to the breast cancerous cell line with the maximum sensitivity of 1.8×10^{10} for T47D ($K = 32$) at $V_{GS} = 0.4$ V.

C. Impact of Geometric Parameter Variation on the Device Sensitivity

In this section, the impact of crucial geometric parameters of the device, such as cavity length (L_1) and FE thickness (t_{FE}), has been investigated on the device sensitivity parameters in terms of drain current sensitivity (S_{ID}), I_{ON}/I_{OFF} sensitivity ($S_{I_{ON}/I_{OFF}}$), transconductance sensitivity (S_{g_m}), and threshold voltage sensitivity ($S_{V_{th}}$). To measure the sensitivity, two cells are utilized, such as nontumorigenic cell line (MCF-10A) and cancerous cell (MDA-MB-231). The cavity length (L_1) has been considered in the range of 20–30 nm to evaluate the impact on sensitivity parameters. Fig. 11(a) and (b) shows the variation in S_{I_D} and $S_{I_{ON}/I_{OFF}}$ by increasing the cavity length of the device, respectively. Moreover, rise in cavity length

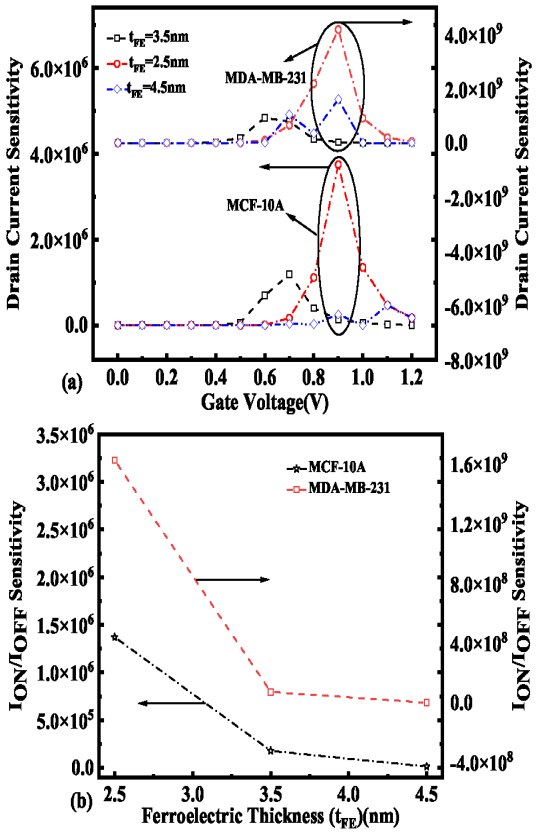

Fig. 13. Impact of FE thickness variation on (a) drain current sensitivity and (b) I_{ON}/I_{OFF} sensitivity of DL-FE-TFET-based biosensor for nontumorigenic (MCF-10A) and cancerous cell (MDA-MB-231).

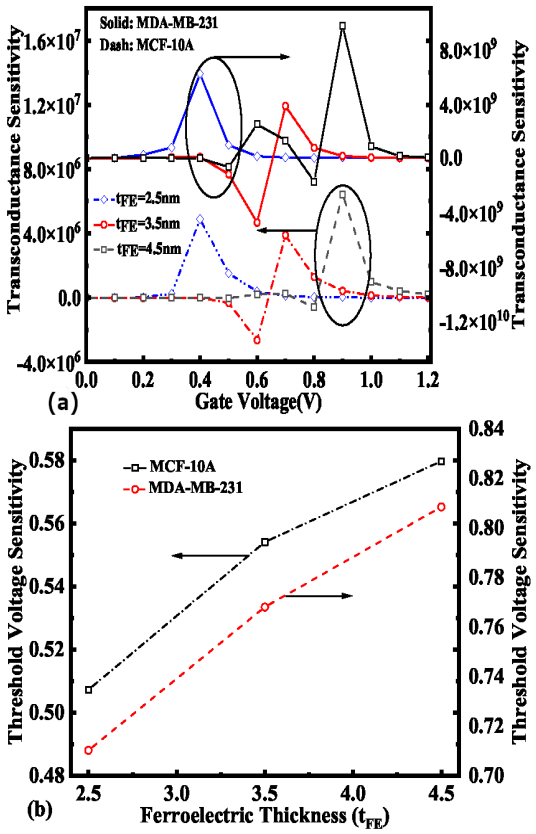

Fig. 14. Impact of FE thickness variation on (a) transconductance sensitivity and (b) threshold voltage sensitivity of DL-FE-TFET-based biosensor for nontumorigenic (MCF-10A) and cancerous cell (MDA-MB-231).

reduces the capacitive coupling between gate electrode and channel region, which results in degraded drive current. Thus, rise in cavity length reduces both S_{I_D} and $S_{I_{ON}/I_{OFF}}$, as shown in Fig. 11. Moreover, Fig. 12 shows the impact of cavity length (L_1) variation on S_{g_m} and $S_{V_{th}}$. It is observed that greater sensitivity achieved for the MDA-MB-231 compared to MCF-10A for both S_{g_m} and $S_{V_{th}}$ and also S_{g_m} increased with an increase in cavity length at lower gate voltage, whereas, with an increase in cavity length, threshold voltage sensitivity decreases.

Furthermore, the impact of variation of FE thickness on the device sensitivity parameter in terms of drain current sensitivity, I_{ON}/I_{OFF} sensitivity, transconductance sensitivity, and threshold voltage sensitivity has been investigated. The FE thickness has been considered a range from 2.5 to 3.5 nm to evaluate the impact on S_{I_D} and $S_{I_{ON}/I_{OFF}}$, as shown in Fig. 13(a) and (b), respectively. Effectively, there are two factors t_{FE} governing NC and the net dielectric layer thickness governing tunneling. Hence, an increase in t_{FE} results in reduced drive current due to poor gate control over channel region as a higher effective increase in dielectric layer thickness is also there. The proposed structure has been utilized for breast cancer cell detection with the binding site beneath the gate electrode. Hence, the increase in t_{Fe} modulates the cavity height, which reduces the gate electrode coupling with the channel region. This effect is more dominant here as there in empty nanocavity also considered here. Thus, it results in a reduced tunneling rate as well as ON state current. Hence, with an increase in t_{FE}, both the sensitivity parameters such as S_{I_D} and $S_{I_{ON}/I_{OFF}}$ decrease, as shown in Fig. 13(a) and (b), respectively. S_{g_m} and $S_{V_{th}}$ variation with an increase in t_{FE} are shown in Fig. 14(a) and (b), respectively. Both S_{g_m} and $S_{V_{th}}$ decrease with an increase in t_{FE} although it can also be noted that enhanced sensitivity is achieved for the MDA-MB-231 compared to MCF-10A.

D. Impact of Biomolecule Occupancy in Cavity Region on Drain Current and I_{ON}/I_{OFF} Sensitivity

Dual underlap cavity underneath gate metal formed as the binding site for the immobilization of the breast cancer cell lines. Cavity regions are considered to be completely filled for the detection of biomolecules. However, it is observed that while biomolecule immobilization, cavity regions are partially filled with the target biomolecule and so have certain vacant spaces. Since the presence of these vacant space in the cavity region for different target biomolecules will change the electrical performance parameters of the proposed device from the expected values, this introduces to another parameter, which can affect the sensitivity named biomolecule occupancy (γ Bio) factor in the underlap cavity region. γ Bio defined as the fraction of cavity region filled with biomolecules (in %) and is described as follows:

$$\gamma_{\text{Bio}} = \frac{\text{Thickness of cavity filled}}{\text{Total thickness of cavity}} \times 100. \quad (6)$$

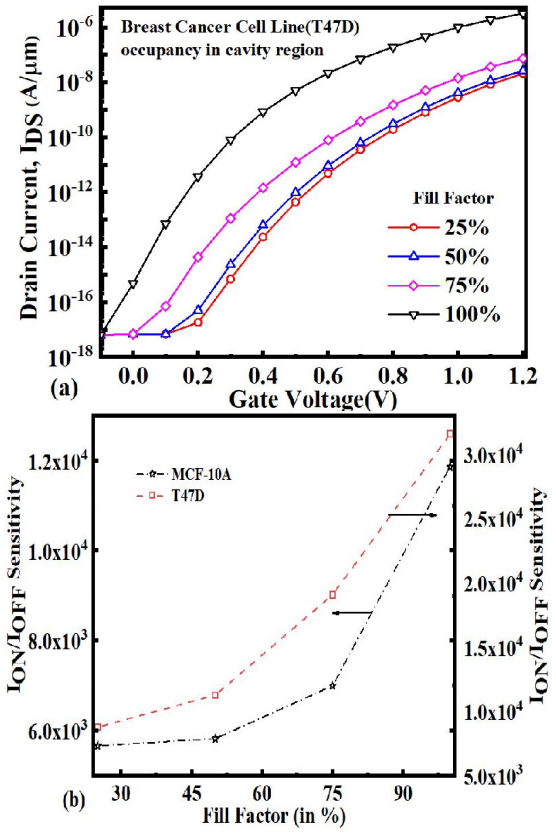

Fig. 15. Impact of fill factor on (a) I_D–V_{GS} characteristic for breast cancer cell line T47D ($K = 32$) and (b) I_{ON}-to-I_{OFF} sensitivity of DL-FE-TFET-based biosensor for nontumorigenic MCF-10A ($K = 4.5$) and cancerous cell T47D ($K = 32$).

Fig. 15(a) shows the variation in the I_D–V_{GS} characteristic of the DL-FE-TFET having cavity thickness as 3 nm for breast cancer cell line (T47D) for different possible arrangements of the biomolecules in the cavity region. For investigating the biomolecules occupancy of device, four points, i.e., 25%, 50%, 75%, and 100%, have been analyzed. To investigate the influence of biomolecule fill factor in cavities, a portion of the cavity is occupied by biomolecules, while the rest is left empty or filled with air. The increase in fill factors (in %) leads to an increase in the biomolecules occupancy due to increase in effective dielectric/capacitance in the cavity region. Thus, it can be noted that drain current increases with fill factor.

The I_{ON}/I_{OFF} sensitivity variation of MCF-10A ($K = 4.5$) and T47D ($K = 32$) with fill factor of cavity region is shown in Fig. 15(b). It is evident that the I_{ON}/I_{OFF} sensitivity of T47D ($K = 32$) is higher and achieved 3×10^4 as maximum value due to its higher dielectric constant.

IV. Conclusion

Breast cancer cell lines (MDA-MB-231, Hs578T, T47D, and MCF-7) detection has been investigated by deploying dopingless NC FE tunnel field-effect transistor (DL-FE-TFET). The dielectric charge modulation effect-based detection of four different types of breast cancer cell lines and nontumorigenic cell lines is reported here. The basic mechanism for breast cancer detection is the immobilization of the breast cancer cell lines in the etched nanocavities beneath the gate metal and the change in the sensitivity parameters after cancerous tissues immobilization are calibrated for the breast cancer cell lines detection. The sensitivity for breast cancer cell lines has been analyzed in terms of drive current, I_{ON}/I_{OFF} ratio, threshold voltage (V_{th}), and transconductance (g_m). The maximum sensitivity achieved is of the order of 1.8×10^{10} for T47D ($K = 32$) at $V_{GS} = 0.4$ V in terms of S_{g_m}. Furthermore, for attaining high sensitivity, cavity length and FE thickness play a very crucial role. Thus, these parameters have been optimized at suitable biasing conditions. The reported device has a simpler transduction mechanism, lower cost, technical compatibility with the CMOS process, tunable electrical responsiveness, and repeatability. This enables it as a strong potential contender for future *in vivo* breast cancer diagnostics.

References

[1] *The Global Cancer Observatory, Age Standardized (World) Incidence Rates, Breast, All Ages*, GLOBOCAN, World Health Organization, 2018.

[2] P. T. Huynh, M. Jarolimek, and S. Dayee, "The false-negative mammogram," *Radiography*, vol. 18, no. 5, pp. 1137–1154, 1998.

[3] J. G. Elmore, M. B. Barton, V. M. Moceri, S. Polk, P. J. Arena, and S. W. Fletcher, "Ten-year risk of false positive screening mammograms and clinical breast examinations," *New England J. Med.*, vol. 338, no. 16, pp. 1089–1096, Apr. 1998.

[4] American Cancer Society. (2007). *Cancer Facts and Figures*. [Online]. Available: https://www.cancer.org

[5] P. Skaane, S. Hofvind, and A. Skjennald, "Randomized trial of screen-film versus full-field digital mammography with soft-copy reading in population-based screening program: Follow-up and final results of Oslo II study," *Radiology*, vol. 244, no. 3, pp. 708–717, Sep. 2007.

[6] P. A. Carney *et al.*, "Individual and combined effects of age, breast density, and hormone replacement therapy use on the accuracy of screening mammography," *Ann. Internal Med.*, vol. 138, no. 3, pp. 168–175, Feb. 2003.

[7] S. J. Lord *et al.*, "A systematic review of the effectiveness of magnetic resonance imaging (MRI) as an addition to mammography and ultrasound in screening young women at high risk of breast cancer," *Eur. J. Cancer*, vol. 43, no. 13, pp. 1905–1917, Sep. 2007.

[8] M. Al-Foheidi, M. M. Al-Mansour, and E. M. Ibrahim, "Breast cancer screening: Review of benefits and harms, and recommendations for developing and low-income countries," *Med. Oncol.*, vol. 30, no. 2, Jun. 2013, Art. no. 471.

[9] U. M. Pal *et al.*, "Optical spectroscopy-based imaging techniques for the diagnosis of breast cancer: A novel approach," *Appl. Spectrosc. Rev.*, vol. 55, no. 8, pp. 778–804, 2020.

[10] M. Säbel and H. Aichinger, "Recent developments in breast imaging," *Phys. Med. Biol.*, vol. 41, no. 3, pp. 315–368, Mar. 1996.

[11] E. C. Fear, P. M. Meaney, and M. A. Stuchly, "Microwaves for breast cancer detection?" *IEEE Potentials*, vol. 22, no. 1, pp. 12–18, Feb./Mar. 2003.

[12] E. C. Fear and M. A. Stuchly, "Microwave detection of breast cancer," *IEEE Trans. Microw. Theory Techn.*, vol. 48, no. 11, pp. 1854–1863, Nov. 2000.

[13] S. C. Hagness, A. Taflove, and J. E. Bridges, "Three-dimensional FDTD analysis of a pulsed microwave confocal system for breast cancer detection: Design of an antenna-array element," *IEEE Trans. Antennas Propag.*, vol. 47, no. 5, pp. 783–791, May 1999.

[14] G. Bindu, S. Abraham, C. K. Aanandan, and K. T. Mathew, "Microwave characterization of female human breast tissues," in *Proc. 9th Eur. Conf. Wireless Technol.*, Sep. 2006, pp. 123–126.

[15] E. C. Fear, X. Li, S. C. Hagness, and M. A. Stuchly, "Confocal microwave imaging for breast cancer detection: Localization of tumors in three dimensions," *IEEE Trans. Biomed. Eng.*, vol. 49, no. 8, pp. 812–822, Aug. 2002.

[16] S. Chaudhary, R. Mishra, A. Swarup, and J. Thomas, "Dielectric properties of normal and malignant human breast tissues at radiowave and microwave frequencies," *Indian J. Biochem. Biophys.*, vol. 21, no. 1, pp. 76–79, 1981.

[17] T. Kim, J. Oh, B. Kim, J. Lee, S. Jeon, and J. Pack, "A study of dielectric properties of fatty, malignant and fibro-glandular tissues in female human breast," in *Proc. Asia–Pacific Symp. Electromagn. Compat.*, Singapore, May 2008, pp. 216–219.
[18] W. T. Joines, Y. Zhang, C. Li, and R. L. Jirtle, "The measured electrical properties of normal and malignant human tissues from 50 to 900 MHz," *Med. Phys.*, vol. 21, no. 4, pp. 547–550, 1994.
[19] D. Sarkar and K. Banerjee, "Proposal for tunnel-field-effect-transistor as ultra-sensitive and label-free biosensors," *Appl. Phys. Lett.*, vol. 100, no. 14, Apr. 2012, Art. no. 143108.
[20] L. Lattanzio, G. A. Salvatore, and A. M. Ionescu, "Non-hysteretic ferroelectric tunnel FET with improved conductance at Curie temperature," in *Proc. 68th Device Res. Conf.*, Jun. 2010, pp. 67–68.
[21] S. Singh and P. N. Kondekar, "Circuit performance and sensitivity analysis of charge plasma based super-steep negative capacitance junctionless tunnel field effect transistor," *J. Nanoelectron. Optoelectron.*, vol. 12, no. 5, pp. 442–451, May 2017.
[22] S. Singh, P. Pal, and P. N. Kondekar, "Charge-plasma-based super-steep negative capacitance junctionless tunnel field effect transistor: Design and performance," *IET Electron. Lett.*, vol. 50, no. 25, pp. 1963–1965, 2014.
[23] M. J. Kumar and S. Janardhanan, "Doping-less tunnel field effect transistor: Design and investigation," *IEEE Trans. Electron Devices*, vol. 60, no. 10, pp. 3285–3290, Oct. 2013.
[24] M. Hussein, F. Awwad, D. Jithin, H. El Hasasna, K. Athamneh, and R. Iratni, "Breast cancer cells exhibits specific dielectric signature *in vitro* using the open-ended coaxial probe technique from 200 MHz to 13.6 GHz," *Sci. Rep.*, vol. 9, no. 1, pp. 1–8, Dec. 2019.
[25] R. Goswami and B. Bhowmick, "Comparative analyses of circular gate TFET and heterojunction TFET for dielectric-modulated label-free biosensing," *IEEE Sensors J.*, vol. 19, no. 21, pp. 9600–9609, Nov. 2019.
[26] A. Saeidi, A. Biswas, and A. M. Ionescu, "Modeling and simulation of low power ferroelectric non-volatile memory tunnel field effect transistors using silicon-doped hafnium oxide as gate dielectric," *Solid-State Electron.*, vol. 124, pp. 16–23, Oct. 2016.
[27] S. Anand and R. K. Sarin, "Dual material gate doping-less tunnel FET with hetero gate dielectric for enhancement of analog/RF performance," *J. Semicond.*, vol. 38, no. 2, Feb. 2017, Art. no. 024001.
[28] *ATLAS, Device Simulation Software*, Silvaco Int., Santa Clara, CA, USA, 2021.
[29] R. Vishnoi and M. J. Kumar, "Compact analytical drain current model of gate-all-around nanowire tunneling FET," *IEEE Trans. Electron Devices*, vol. 61, no. 7, pp. 2599–2603, Jul. 2014.
[30] A. Singh, R. Narang, M. Saxena, and M. Gupta, "Analytical modeling of a split-gate dielectric modulated metal-oxide-semiconductor field-effect transistor for application as a biosensor," in *Proc. 2nd Int. Conf. Devices, Circuits Syst. (ICDCS)*, Mar. 2014, pp. 1–6.
[31] S. Singh, P. N. Kondekar, and N. K. Jaiswal, "Label-free biosensor using nanogap embedded dielectric modulated Schottky tunneling source impact ionization MOS," *Microelectron. Eng.*, vol. 149, pp. 129–134, Jan. 2016.
[32] G. Wadhwa and B. Raj, "Parametric variation analysis of symmetric double gate charge plasma JLTFET for biosensor application," *IEEE Sensors J.*, vol. 18, no. 15, pp. 6070–6077, Aug. 2018.
[33] S. Singh and S. Singh, "Analog/RF performance projection of ultra-steep Si doped HfO_2 based negative capacitance electrostatically doped TFET: A process variation resistant design," *Silicon*, pp. 1–13, Jul. 2021.
[34] M. Azizi, H. Ghourchian, F. Yazdian, S. Bagherifam, S. Bekhradnia, and B. Nyström, "Anti-cancerous effect of albumin coated silver nanoparticles on MDA-MB 231 human breast cancer cell line," *Sci. Rep.*, vol. 7, no. 1, pp. 1–18, Dec. 2017.
[35] K. Venugopal *et al.*, "Synthesis of silver nanoparticles (Ag NPs) for anticancer activities (MCF 7 breast and A549 lung cell lines) of the crude extract of *Syzygium aromaticum*," *J. Photochem. Photobiol. B, Biol.*, vol. 167, pp. 282–289, Feb. 2017.
[36] T. T. Hoai *et al.*, "Evaluation of the cytotoxic effect of rutin pre-nanoemulsion in lung and colon cancer cell lines," *J. Nanomater.*, vol. 2020, pp. 1–11, Nov. 2020.
[37] Y. Zhang, M. Li, X. Gao, Y. Chen, and T. Liu, "Nanotechnology in cancer diagnosis: Progress, challenges and opportunities," *J. Hematol. Oncol.*, vol. 12, no. 1, pp. 1–13, Dec. 2019.

Shradhya Singh received the M.Tech. degree in VLSI design from the Dr. B. R. Ambedkar National Institute of Technology Jalandhar, Jalandhar, Punjab, India, in 2017. She is currently pursuing the Ph.D. degree with the Electronics and Communication Department (VLSI Design), National Institute of Technology at Patna, Patna, Bihar, India.

Her current research interests include the area of modeling and of nano scale semiconductor device, doping-less negative capacitance TFET for biosensing application.

Sangeeta Singh (Member, IEEE) received the Ph.D. degree in electronics and communication engineering from PDPM-Indian Institute of Information Technology, Design and Manufacturing, Jabalpur, India.

She is currently an Assistant Professor with the Department of Electronics and Communication Engineering, National Institute of Technology (NIT) at Patna, Patna, India. She has been recognized as an eminent scholar in the field of electronics engineering. She has published many research papers in reputed national/international journals and conferences.